Article

Combustion Inhibition of Aluminum–Methane–Air Flames by Fine NaCl Particles

Wu Xu and Yong Jiang *

State Key Laboratory of Fire Science, University of Science and Technology of China, Hefei 230027, China; xuwu0618@ustc.edu.cn

* Correspondence: yjjiang@ustc.edu.cn; Tel.: +86-551-63607827

check for updates

Abstract: The effect of NaCl as an extinguishing agent on metal dust fires require further exploration. This paper reports the results of an experimental study on the performance of micron-sized NaCl powders on hybrid aluminum–methane–air flames. NaCl particles with sub-10 μm sizes were newly fabricated via a simple solution/anti-solvent method. The combustion characteristics of aluminum combustion in a methane-air flame were investigated prior to the particle inhibition study to verify the critical aluminum concentration that enables conical aluminum-powder flame formation. To study the inhibition effectiveness, the laminar burning velocity was measured for the established aluminum–methane–air flames with the added NaCl using a modified nozzle burner over a range of dust concentrations. The results were also compared to flames with quartz sand and SiC particles. It is shown that the inhibition performance of NaCl considerably outperformed the sand and SiC particles by more rapidly decreasing the burning velocity. The improved performance can be attributed to contributions from both dilution and thermal effects. In addition, the dynamic behavior of the NaCl particles in the laminar aluminum–methane–air flame was investigated based on experimental observations. The experimental data provided quantified the capabilities of NaCl for metal fire suppression on a fundamental level.

1. Introduction

Prevention of dust explosions is of great scientific and practical interest because micron- or nano-sized particles when dispersed in the form of a cloud, present a real threat to processing industries and to humans [1,2]. Sometimes, these particles are entrained by a combustible gas, resulting in two-phase hybrid mixture combustion. Generally, it has been experimentally confirmed that a hybrid of solid and gaseous fuel has a lower flammability limit, a higher energy density and can be easily ignited by a very small ignition energy compared with that of dust–air systems [3,4]. Earlier studies relating to explosions of hybrid mixtures and their suppression have mainly focused on the mining industry with coal dust mixing with methane gas as the research focus [5,6]. Since metal dust is encountered in numerous modern technological applications [7,8], as well as in numerous fatal explosions, specific research on the suppression of metal dust fires is required and is the topic of the current study.

Laminar burning velocity (LBV) is an intrinsic property of any premixed reacting mixture, and it is a measure of the mixture's exothermicity, diffusivity and overall reactivity in combustion [9,10]. Studies on the propagation and mitigation of aluminum dust flames that are available in the literature have mostly been conducted in closed standard spherical vessels where the combustion characteristics, such as the ignition energy and explosion pressure rise, have been investigated. Denkevits and

Hoess [11] used a 20 L spherical vessel to study the explosion behavior of hybrid mixtures of 1 μm aluminum dust/hydrogen/air. Recently, Jiang et al. [12]. studied the suppression performance of $NaHCO_3$ on an aluminum dust explosion in a similar spherical chamber and reported that the minimum inerting concentration (MIC) for the explosion of 5 μm aluminum is higher than that of 30 μm. The size distribution of the commercial $NaHCO_3$ powder is in the range of 53–212 μm in Reference [10]. Taveau et al. [13] reviewed suppression experiments on metal dusts on different scales. To our knowledge, few studies of LBV measurements have been performed for metal dust and, particularly, aluminum combustion has not been studied until very recently. Sikes et al. [14] attempted to measure the LBV of oxygen-enriched nano-aluminum/methane hybrid mixtures using a combustion vessel apparatus with a refined injection unit to obtain a uniformly dispersed aerosol. In their study, however, the seeding amount of aluminum was on the trace level, which was lower than ~3.5 g/m^3. Julien et al. [15] built a counterflow particulate-fuel burner and used it to measure the burning velocities of aluminum/air mixtures but did not eliminate the flame stretch. In contrast to gaseous or liquid fuels, this revealed that there are challenges in LBV measurements of mixtures in the presence of solid particulates via conventional techniques, such as using counterflow flames [16], spherically expanding flames [17], or flat flames [18]. To determine the burning velocity of particulate fuels, a conical Bunsen flame technique was used by WPI researchers [5,19–21]. This common approach has proven to be adequate if the deviations caused by the stretch effects are fully assessed [22]. To continue this effort, this paper introduces a new hybrid flame burner for LBV measurements of gas and gas–solid fuel premixed flames.

The suppression of metal fires using inert dusts, such as sand, has been commonly used for a very long time [23]. Sand particles, however, have practical application limitations associated with particle delivery and storage issues. Currently, although some new agents have been identified as effective fire suppressants (e.g., halon replacements and water mist), the incorrect application of inhibitors for suppressing metal fires can cause an enhancement effect on the system due to exothermic reactions of metal with either or both the inhibitor and products. Sodium chloride (NaCl), which now serves as the main effective substance in portable fire extinguishers for class D (combustible metals) fires, has many advantages as it is not rare, it is environmentally benign, and has a relatively high heat capacity [24,25]. In terms of the inhibition mechanism, sodium chloride particles generally act as an inert inhibitor via the two following physical inhibition mechanisms: (1) a thermal effect associated with heat absorption and the latent heat of vaporization and (2) a dilution effect induced by the decrease in the reactant concentration. For a specific application, detailed quantitative information understanding the performance of NaCl particles on metal fires is useful for designing and optimizing these particles. Fundamentally, this requires an investigation of the burning velocity retardation by NaCl particles; however, no study available in the literature has attempted to explore its impact on flame propagation to quantify the effectiveness of NaCl for flame inhibition.

In this work, NaCl particles were prepared using a solution/anti-solvent method in our laboratory. Improvements in the hydrophobicity and dispersivity were achieved by introducing hydrophobic nano-SiO_2 (silicon dioxide) attached to the surface of the NaCl particles. The objectives of this study were to estimate the flame propagation velocity inhibition by adding NaCl in a hybrid mixture of aluminum and methane and to study the performance of the newly fabricated micron-sized NaCl particles. The arrangement of this paper is as follows: the methods for preparing the micron-sized NaCl powders and for the characterization of aluminum and NaCl are presented first. The laminar burning velocities of the aluminum–methane–NaCl–air mixtures were determined using conical flame experiments. Finally, the results are concluded with a few comments.

2. Experimental Methods

2.1. Experimental Apparatus and Procedures

The hybrid fuel combustion experiments were conducted in an axisymmetric stainless-steel burner. An overview of the newly constructed experimental setup is shown in Figure 1. The design of the burner implemented several technical solutions considered previously in the building of nozzle burners [26,27]. In particular, it used a profiled converging nozzle to reduce the boundary layer thickness and to yield a top-hat (plug-flow) velocity profile at the exit plane. Specifically, the axial velocity of the cold flow that was measured using a hot-wire anemometer (Kanomax 6162, KANO Co., Ltd, Shenyang, China), is shown in Figure 2, indicating a quite flat velocity profile across over 70% of the exit plane. The contoured nozzle had an outlet diameter of d = 10 mm, and the contraction ratio was $\sigma = (D/d)^2 = 16$. High purity nitrogen was supplied surrounding the nozzle to shield the combustible mixture from the ambient environment. The burner inner face was finely polished to minimize disturbances to the flow due to irregularities. To prevent overheating, the nozzle was water-cooled to keep the outlet mixture at the ambient temperature.
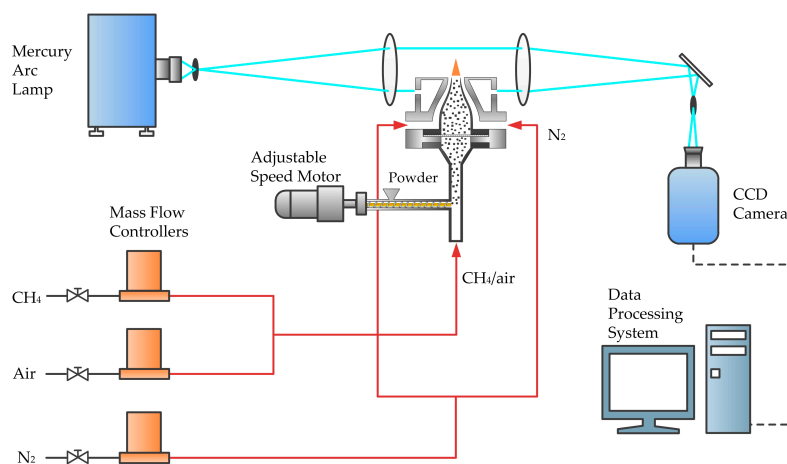
Figure 1. Schematic of the experimental setup for the premixed hybrid fuel combustion.
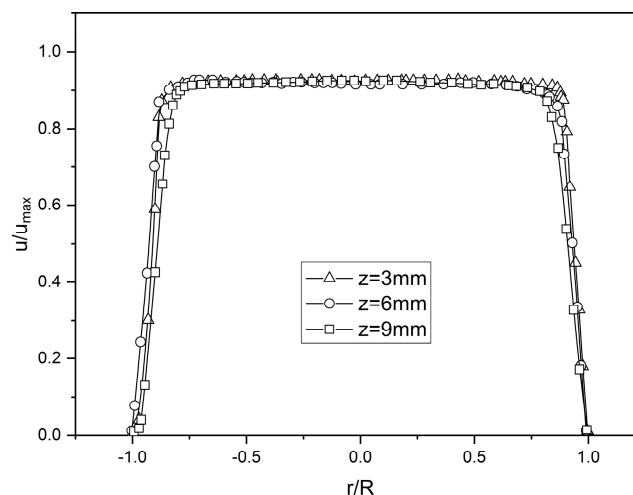

Figure 2. Normalized axial velocity u/u_{max} (u_{max} = 1.5 m/s) as a function of normalized radial distance r/R measured at variousaxial distance (z = 3, 6, and 9 mm).

Methane (purity > 99.99%) and synthetic air (21% O_2 in N_2), provided by the Nanjing Special Gas Factory (Nanjing, China) were employed as the fuel gas and oxidizer, respectively. The flow rates were

metered by MKS mass flow controllers that were periodically calibrated against a digital soap film flowmeter (stated accuracy of $\pm0.5\%$ for the reading).

The methane/air mixture flow acts as the aluminum particle carrier gas. After a group of test runs, the volumetric flow rate of the carrier gas was fixed at 5.5 standard liters per minute (SLPM, at 0 °C and 1 atm). During the experiments, the burner assembly and pipelines were heated using a ceramic heating jacket and heating types. A K-type thermocouple was placed immediately downstream of the burner exit to monitor the T_u of the combustible mixture, which was maintained at ambient temperature (T_u =298 $\pm$ 3 K). The particle samples were continuously fed to the main jet using a screw feeder, which is an assembly of the following components: a homemade helical screw, a feed hopper with a vibrator and an adjustable speed motor with a digital speed controller. As a result of the continuity of the flow, the dust entrained into the methane-air stream, creating a hybrid mixture. A 100 mesh (aperture size of 0.154 mm) screen that was installed at the bottom of the converging nozzle was utilized to dampen the turbulence of the hybrid mixture and to homogeneously disperse the particles. As the flow continuously passes through the screen, dust particles may deposit on the screen mesh, causing a local blockage and hence a flow instability may be transmitted to the burner outlet. Therefore, additional care was taken to prevent this and the dust deposition was neglected if each experiment could be finished in 2 min. Figure 3 displays images of the aluminum particles as they exited the burner illuminated with a 1.5 mm-thick laser sheet at different aluminum concentrations. The powder feed rate was determined by a direct calibration procedure. A vacuum pump was used to aspirate the dusty flow through a probe that contained quartz wool for a certain flow volume; the deposited dust was then weighted and a calibration curve was obtained based on the variation of the rotary screw speed. The particle mass loading was determined by dividing the total volume of the solid–gas mixture by the mass of the particles that passed through the mesh screen during a given time interval.
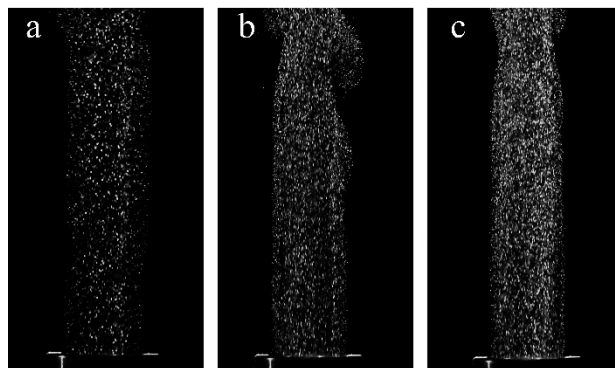
Figure 3. Photographs of laser-illuminated Al particles at different concentrations: (**a**) 12 g/m^3, (**b**) 55 g/m^3, and (**c**) 152 g/m^3. The exposure time of the camera was 1/8000 s.

Visualization of the flame was achieved using a transmission Schlieren apparatus. A high-intensity discharge mercury arc lamp (power of 100 W, wavelength of 200–2500 nm) was employed as the light source for the illumination. A collimated light beam was formed using a pinhole (diameter of 200 mm) placed at the focal point of a plano-convex lens attached to the lamp housing and an achromatic Fourier transform lens (diameter of 100 mm, focal length of 400 mm). After travelling through the flame region and a second identical achromatic Fourier transform lens (diameter of 100 mm, focal length of 400 mm), the collimated light beam was focused on an adjustable iris diaphragm (aperture of 0.8–7.5 mm). Schlieren images were recorded via a high-resolution CCD camera at 10 frames per second. The visual flame chemiluminescence images were taken using a digital single lens reflex (DSLR) camera.

Laminar burning velocity measurements of the burner stabilized flame were performed based on the law of mass conservation. The well-established flame cone angle [28–31] and flame surface

area [32,33] approaches have been developed to determine the laminar burning velocity S_u^0. In the first technique, the velocity component normal to the flame front is locally equal to the propagation velocity of the flame front, which is interpreted as the laminar burning velocity relative to the unburnt mixture; therefore, the experimental S_u^0 can be calculated by Equation (1):

$$S_u^0 = u_0 \cdot \sin \alpha \qquad (1)$$

where u_0 is the bulk velocity of the unburned mixture, and α is the half cone angle of the flame.

Conical flames are known to be affected by a series of inherent problems, such as a strong curvature at the flame tip, strain along the flame sides and heat losses to the burner that cause local quenching at the flame base. Modifications to the burning velocity due to these effects can be minimized by implementing technical solutions to achieve reasonable levels of measurement accuracy. In our experimental method, an aerodynamically contoured nozzle was used to generate fairly straight-sided flame cones, which ensured that the flame propagated uniformly towards the unburned mixture over the main part of the flame zone [34,35]. The heat losses at the burner rim were assumed to be small, considering that the thickness of the nozzle wall was reduced and only a small portion of the flame border was close to the burner rim. Previous demonstrations of this laminar burning velocity measurement approach have been performed for both gaseous [30,35,36] and hybrid gas-solid mixtures [19,37], demonstrating that the conical flame method is very accurate by considerably reducing the effects of flame stretch and curvature.

Figure 4 depicts the conical flame analysis procedure. Figure 4a shows a typical visual image of a hybrid methane–aluminum–air flame. Each available Schlieren image was averaged from a set of approximately 30 instantaneous Schlieren images of the conical flame, as shown in Figure 4b. Then, the edge of the time-averaged flame was derived by an automatic image processing program based on the Sobel operator in a Matlab environment, as shown by the black symbols in Figure 4c. A linear fitting algorithm was applied to the continuity points that characterized the flame edge; then, slopes of the fitted lines from the sides of the cone were calculated, denoted as k_1 and k_2, also shown in Figure 4c. The half cone angle of the flame can be obtained from $\alpha = \left[\tan^{-1}(k_1) + \tan^{-1}(k_2)\right]/2$. Using this procedure, the calculated burning velocity matches closely with literature data, as discussed in Section 3.
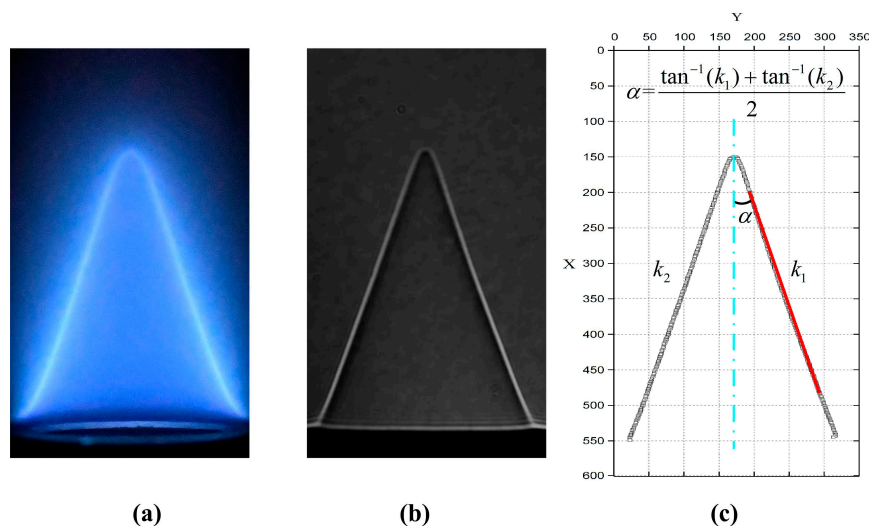
Figure 4. Flame image processing. (**a**) Methane/air flame, (**b**) Schlieren photography, and (**c**) a processed image.

An experimental uncertainty analysis was performed for the LBV measurement using the equation that was outlined by Moffat [38]: $\delta_{S_u^0} = \sqrt{\left(B_{S_u^0}\right)^2 + \left(t S_{S_u^0}/\sqrt{N}\right)^2}$, where $\delta_{S_u^0}$ is the overall uncertainty

for the measured S_u^0, $B_{S_u^0}$ is the total bias uncertainty, $S_{S_u^0}$ is the standard deviation of N repeated experiments, and t is the Student's multiplier for 95% confidence and $N - 1$ degrees of freedom. The relative combined overall uncertainties of the measurements could be associated with each measured component, i.e., initial temperature, flame surface recognition and data analysis. The relative overall uncertainties of ϕ arise from the measurement of CH_4 and the air flow rates were estimated to be 1–2%.

2.2. Materials and Sample Preparation

A typical experiment for the preparation of NaCl dry powder was as follows. (1) First, 100 g of sodium chloride (AP, NaCl, Sinopharm Group Co., Ltd, Shanghai, China) and deionized water were mixed as a saturated solution. The initial NaCl solution pH was adjusted by 1.0 M hydrochloric acid for the desired value of 1.0 during rapid magnetic stirring. Then, a certain amount of polyethylene glycol (AP, PEG1000, Sinopharm Group Co., Ltd.) was added to the above solution at a temperature of 60 °C. (2) We added 0.1 mass% of hydrophobic SiO_2 nanoparticles (>99.8% purity, Shanghai Macklin Biochemical Co., Ltd, Shanghai, China) to 400 mL of anhydrous alcohol in a 3-neck round bottom flask and conducted ultrasound treatment for 0.5 h. Afterwards, the as-prepared NaCl solution was rapidly injected into the dispersed SiO_2 sol. Vacuum filtration was implemented for the NaCl slurry and water was removed by anhydrous alcohol washing. The powder samples were dried under vacuum at 100 °C for 4 h prior to further analysis.

2.3. Structural Characterization

The particle size distributions of the Al powder and newly fabricated NaCl samples were detected using isopropyl alcohol as the dispersing medium in a Mastersizer 3000E laser particle analyzer (Malvern Panalytical Co., Ltd, Malvern, UK). Phase identifications were determined by X-ray diffraction (XRD, X'Pert Pro, Malvern PANalytical Co., Ltd, Malvern, UK). A scanning electron microscope (SEM, Gemini 500, ZEISS Co., Ltd, Jena, Germany) was used to observe the surface morphology of the samples.

3. Results and Discussion

3.1. Particle Characterization

The X-ray diffraction (XRD) pattern of the as-prepared NaCl particles, using the solution/anti-solvent method is shown in Figure 5. The XRD pattern exhibits sharp diffraction peaks, which is in accordance with the standard NaCl pattern. This indicates the high crystallization integrity of the particles.
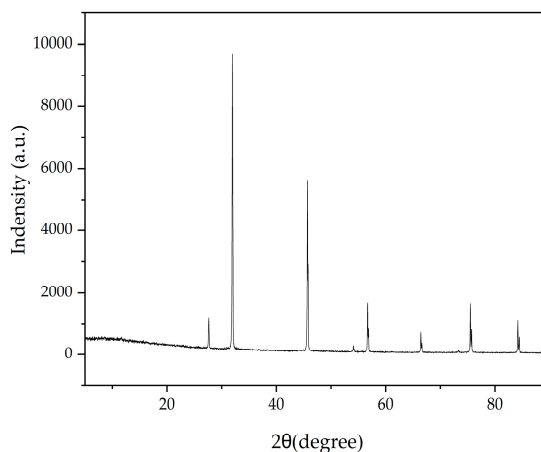
Figure 5. XRD of sodium chloride prepared by the solution/anti-solvent crystallization method.

Figure 6 shows representative SEM images of the aluminum and sodium chloride particles. Aluminum submicron particles with a stated purity of 99.9% and a fundamental size of 800 nm, were purchased from Beijing DK Nano Technology Co., Ltd. (Beijing, China). The as-received particles were of a spherical shape and the degree of particle agglomeration was much lower than nano-sized aluminum (80 nm) also produced by the DK Company [39] (Figure 6a). Figure 6b shows the micromorphology of the NaCl particles, indicating a regular cubic structure with very small quantities of SiO_2 (d = 20 nm) adhering to the surface of each individual cube. The tiny SiO_2 particles improve the powder flowability but made no difference to the experimental results. The Sauter mean diameters, D_{32}, of the aluminum and NaCl were 0.87 µm and 7.6 µm, respectively (Figure 6).
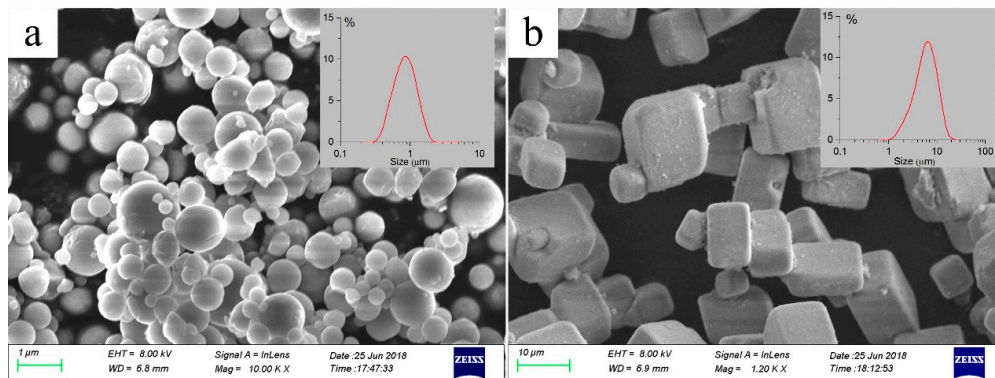
Figure 6. SEM photographs and particle size distributions of (**a**) the aluminum particles and (**b**) the sodium chloride particles.

### 3.2. Gas Flames (Validation Test)

In this study, the laminar burning velocities of pure CH_4/air mixtures were first measured to assess the accuracy of the current experimental setup and data analysis procedures. Experimental verification was performed for the range of equivalence ratios of 0.8–1.4. For leaner flames, flame detachment occurred at even a low flow rate, and the flame could not be stabilized on the burner. Figure 7 compares the current measured LBVs of CH_4/air mixtures with the well-documented datasets of previous measurements from the spherically expanding flame [40–42], the counterflow flame [43] and the heat flux method [44]. The current data are in good agreement with previous results obtained by these independent methodologies and agree reasonably well with the GRI-mech 3.0 model predictions. The comparison results show that the new experimental setup provides accurate measurements of burning velocities by using the cone flame method.
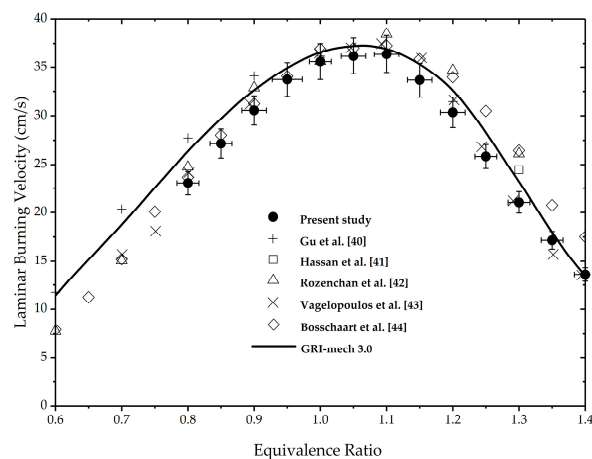
Figure 7. Experimental (symbols) and computed (lines) laminar burning velocities of methane/air mixtures at 298 K and atmospheric pressure.

3.3. Burning Velocities of the Aluminum/Methane/Air Hybrid Mixtures

The effect of the solid aluminum particles on flame propagation in the hybrid mixture of aluminum and methane was investigated for three different aluminum concentration ranges: 10–23, 45–68, and 100–120 g/m^3. Aluminum dust was added to initially stoichiometric ($\phi = 1.0$), lean ($\phi = 0.8$) and rich ($\phi = 1.2$) methane/air mixtures. Figure 8 shows the laminar burning velocity results for the Al/CH$_4$/air experiments. The introduction of aluminum particles reduced the burning velocity of methane for all of the particle concentrations studied with a decreasing marginal effect at higher particle concentrations. For the stoichiometric mixture, the aluminum caused a maximum burning velocity retardation of 6.2 cm/s from the benchmark value of 35.6 cm/s; for the lean and rich mixtures, the maximum decrease was slightly lower at ~5.4 and 2.2 cm/s respectively. Thus, with the solid combustible component suspended in premixed methane/air flames, the mixture became less reactive with a steady decrease in the flame burning velocity. This result is consistent with the decreasing behavior that was experimentally observed by Sikes et al. [14] and Soo et al. [45], where aluminum particles were added to a similar methane/air mixture but investigated with a smaller ($d = 100$ nm) and larger ($d = 5.6$ μm) fundamental particle size. Apparently, aluminum combustion in the hybrid mixture was subjected to a complicated mechanism due to the multiplicity of the thermal physical properties of the solid fuel. When an aluminum particle reaches the combustion zone, it absorbs heat from the methane flame before it burns in the vapor phase. Thus, the particle acts in a similar way as compared to a heat sink, resulting in a decrease in the flame temperature. On the other hand, aluminum particle combustion in a methane flame introduces additional heat release, which would likely increase the burning velocity. It is assumed that the above two competing effects led to the burning velocity trend shown in Figure 8. In fact, it was suspected that as the aluminum particles released volatiles, it could lead to an increase in the overall equivalence ratio, thus making the mixture become richer. However, due to the absence of insufficient oxygen after the methane flame, the aluminum particles mainly reacted with the product gases instead of producing full combustion.
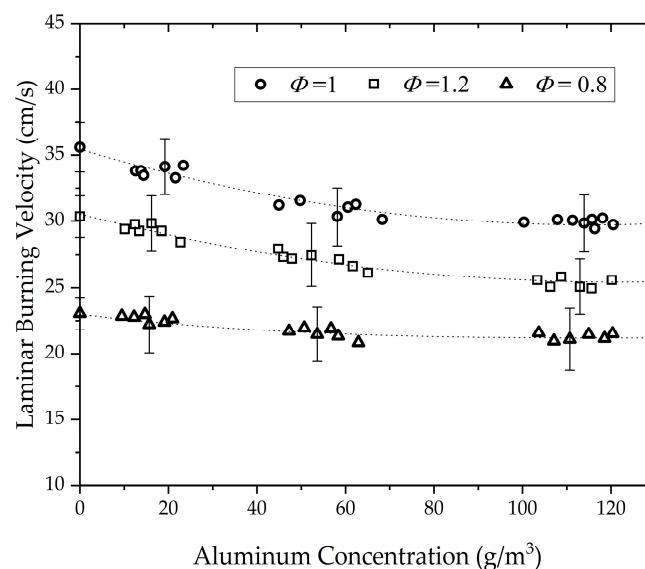

Figure 8. Laminar burning velocities of Al/CH$_4$/air mixtures for different aluminum concentration ranges. For clarity, the dotted lines only represent the data trends.

3.4. Flame Appearance and Flame Front Formation

Figure 9 shows images of the aluminum/methane/air flames for two different aluminum concentrations and a typical image of an inhibited hybrid flame by NaCl particles. For the methane flame with a low aluminum particle loading, only the hydrocarbon flame front was visible (Figure 9a). As more aluminum particles were introduced, the aluminum flame front was formed and was observed

to be coupled to the methane flame front. The local streamline of the individual aluminum particles is clearly visible (Figure 9b). It was observed that the addition of NaCl particles decreased the flame luminous emissions and suppressed the combustion intensity of each aluminum particle because a diffuse glow appeared instead of the particle burning trajectories. During the experiment, it was also found that at higher NaCl concentrations, the flame showed a propensity to become unstable due to diffusive-thermal instabilities. The tip of the flame cone was observed to split at a NaCl concentration of approximately 100 g/m^3, and a small number of particles escaped without fulfilling their useful functions.
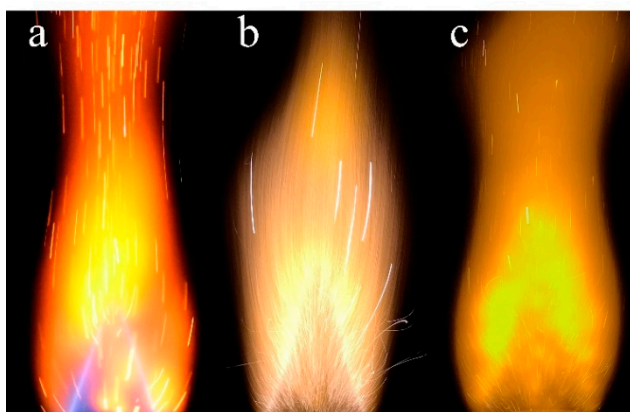
Figure 9. Visual images of the hybrid flames. (**a**) An Al/CH$_4$/air flame with a low Al concentration (10 g/m^3); (**b**) An Al/CH$_4$/air flame with a medium Al concentration (50 g/m^3); (**c**) An Al/CH$_4$/air flame with NaCl added at a medium concentration (50 g/m^3 Al, 50 g/m^3 NaCl).

3.5. Burning Velocities of the Aluminum/Methane/Sodium Chloride/Air Hybrid Mixtures

To investigate the suppression effectiveness of sodium chloride in the hybrid methane/air mixture, burning velocity measurements were performed for the Al/CH$_4$/air flames with increasing amounts of added NaCl particles. The results were also compared to data measured with silicon carbide (SiC, d = 8 μm) and quartz sand particles (d = 10.5 μm). The stoichiometric methane/air with a medium concentration of aluminum was adopted as a baseline because the metal flame front formed in the presence of the medium concentration, indicating that a stabilized metal–powder conical flame was generated and merged with the methane flame, which was a prerequisite to performing the inhibition experiments. As shown in Figure 10, adding each inhibitor reduced the LBV data for all particle concentrations. Since the specific heat of the quartz sand is larger than that of SiC (0.83 versus 0.67 J/g K) and they both simply act as inert particles with a similar particle size, the suppression effectiveness of quartz sand is superior to silicon carbide. Furthermore, the suppression effectiveness of NaCl is significantly better than quartz sand, even though they have a similar value of specific heat (0.86 versus 0.83 J/g K). In fact, in addition to the dilution effect, NaCl particles can efficiently absorb radiation emitted from the reaction zone during the melting process. Furthermore, the melting component was coated on the surface of the aluminum particles excluding air access, which also contributed to the fire suppression.
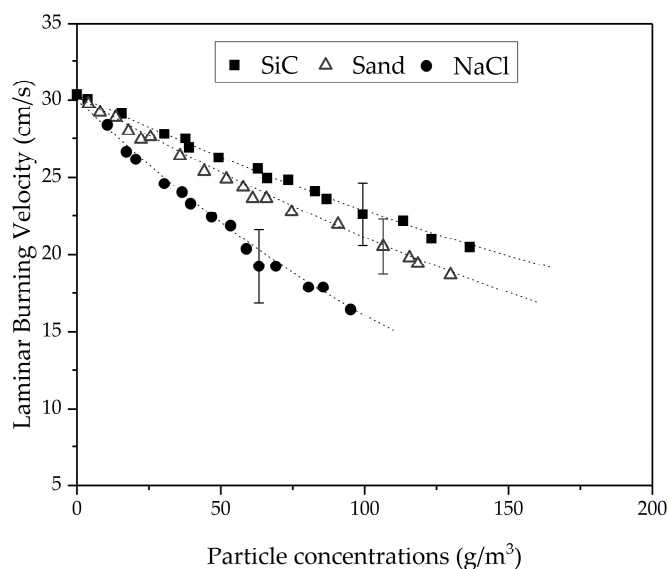
Figure 10. Laminar burning velocities of the Al/CH$_4$/air mixtures with inert particles of NaCl, SiC, or quartz sand. For clarity, the dotted lines only represent the data trends.

4. Conclusions

Aluminum dust-entrained fire is highly dangerous and is difficult to extinguish by conventional fire agents. NaCl is a preferred candidate for handling this specific fire type. In this study, micron-scale NaCl powder was fabricated via a simple solution/anti-solvent method. A modified nozzle burner that was designed to operate with combustible gas–dust hybrid mixtures was used to investigate the effect of NaCl on stabilized aluminum/methane/air flames. Combustion tests were performed using the Schlieren technique by marking the conical flame edge to determine the laminar burning velocity. For pure aluminum/methane/air flames, an aluminum combustion front formed above a certain Al concentration, which can only then represent a stabilized metallic-involved flame. The results indicate that the addition of aluminum submicron particles influenced the methane flame by reducing the flame burning velocity. When the micron-sized NaCl particles were added, the burning velocity considerably decreased with an increasing concentration of NaCl toward the opened end of the flame tip. The suppression effectiveness of NaCl is better than quartz sand and SiC for reducing the burning velocity. This is not only due to the rapid melting of NaCl particles that causes a cooling effect on the flames but is also due to the molten NaCl coating the metal particles, which excluded air access.

References

1. Bouillard, J.; Vignes, A.; Dufaud, O.; Perrin, L.; Thomas, D. Ignition and explosion risks of nanopowders. *J. Hazard. Mater.* **2010**, *181*, 873–880. [CrossRef] [PubMed]
2. Li, G.; Yang, H.X.; Yuan, C.M.; Eckhoff, R.K. A catastrophic aluminium-alloy dust explosion in China. *J. Loss Prev. Process Ind.* **2016**, *39*, 121–130. [CrossRef]
3. Russo, P.; Di Benedetto, A.; Sanchirico, R. Theoretical evaluation of the explosion regimes of hybrid mixtures. *Chem. Eng. Trans.* **2012**, *26*, 51–56.
4. Ajrash, M.J.; Zanganeh, J.; Moghtaderi, B. Effects of ignition energy on fire and explosion characteristics of dilute hybrid fuel in ventilation air methane. *J. Loss Prev. Process Ind.* **2016**, *40*, 207–216. [CrossRef]

5. Xie, Y.; Raghavan, V.; Rangwala, A.S. Study of interaction of entrained coal dust particles in lean methane–air premixed flames. *Combust. Flame* **2012**, *159*, 2449–2456. [CrossRef]

6. Li, Q.; Lin, B.; Dai, H.; Zhao, S. Explosion characteristics of H_2/CH_4/air and CH_4/coal dust/air mixtures. *Powder Technol.* **2012**, *229*, 222–228. [CrossRef]

7. Greatrix, D. Numerical Evaluation of the Use of Aluminum Particles for Enhancing Solid Rocket Motor Combustion Stability. *Energies* **2015**, *8*, 1195–1215. [CrossRef]

8. Taveau, J.; Hochgreb, S.; Lemkowitz, S.; Roekaerts, D. Explosion hazards of aluminum finishing operations. *J. Loss Prev. Process Ind.* **2018**, *51*, 84–93. [CrossRef]

9. Law, C.K. *Combustion Physics*; Cambridge University Press: Cambridge, UK, 2006.

10. Ranzi, E.; Frassoldati, A.; Grana, R.; Cuoci, A.; Faravelli, T.; Kelley, A.P.; Law, C.K. Hierarchical and comparative kinetic modeling of laminar flame speeds of hydrocarbon and oxygenated fuels. *Prog. Energy Combust. Sci.* **2012**, *38*, 468–501. [CrossRef]

11. Denkevits, A.; Hoess, B. Hybrid H_2/Al dust explosions in Siwek sphere. *J. Loss Prev. Process Ind.* **2015**, *36*, 509–521. [CrossRef]

12. Jiang, H.; Bi, M.; Gao, W.; Gan, B.; Zhang, D.; Zhang, Q. Inhibition of aluminum dust explosion by $NaHCO_3$ with different particle size distributions. *J. Hazard. Mater.* **2018**, *344*, 902–912. [CrossRef] [PubMed]

13. Taveau, J.; Vingerhoets, J.; Snoeys, J.; Going, J.; Farrell, T. Suppression of metal dust deflagrations. *J. Loss Prev. Process Ind.* **2015**, *36*, 244–251. [CrossRef]

14. Sikes, T.; Mannan, M.S.; Petersen, E.L. Laminar flame speeds of nano-aluminum/methane hybrid mixtures. *Combust. Flame* **2016**, *166*, 284–294. [CrossRef]

15. Julien, P.; Whiteley, S.; Soo, M.; Goroshin, S.; Frost, D.L.; Bergthorson, J.M. Flame speed measurements in aluminum suspensions using a counterflow burner. *Proc. Combust. Inst.* **2017**, *36*, 2291–2298. [CrossRef]

16. Ji, C.; Dames, E.; Wang, H.; Egolfopoulos, F.N. Propagation and extinction of benzene and alkylated benzene flames. *Combust. Flame* **2012**, *159*, 1070–1081. [CrossRef]

17. Nativel, D.; Pelucchi, M.; Frassoldati, A.; Comandini, A.; Cuoci, A.; Ranzi, E.; Chaumeix, N.; Faravelli, T. Laminar flame speeds of pentanol isomers: An experimental and modeling study. *Combust. Flame* **2016**, *166*, 1–18. [CrossRef]

18. Bosschaart, K.J.; De Goey, L.P.H. Detailed analysis of the heat flux method for measuring burning velocities. *Combust. Flame* **2003**, *132*, 170–180. [CrossRef]

19. Ranganathan, S.; Lee, M.; Akkerman, V.; Rangwala, A.S. Suppression of premixed flames with inert particles. *J. Loss Prev. Process Ind.* **2015**, *35*, 46–51. [CrossRef]

20. Ranganathan, S.; Petrow, D.; Rockwell, S.R.; Rangwala, A.S. Turbulent burning velocity of methane–air–dust premixed flames. *Combust. Flame* **2018**, *188*, 367–375. [CrossRef]

21. Rockwell, S.R.; Rangwala, A.S. Influence of coal dust on premixed turbulent methane–air flames. *Combust. Flame* **2013**, *160*, 635–640. [CrossRef]

22. Bouvet, N.; Chauveau, C.; Gökalp, I.; Lee, S.Y.; Santoro, R.J. Characterization of syngas laminar flames using the Bunsen burner configuration. *Int. J. Hydrogen Energy* **2011**, *36*, 992–1005. [CrossRef]

23. NPFA 484. In *Standard for Combustion Metals*; Naional Fire Protection Association: Quincy, MA, USA, 2009.

24. Roberts, M.; Rogers, W.J.; Sam Mannan, M.; Ostrowski, S.W. Prevention and suppression of metal packing fires. *J. Hazard. Mater.* **2003**, *104*, 247–253. [CrossRef]

25. Zalosh, R. Metal hydride fires and fire suppression agents. *J. Loss Prev. Process Ind.* **2008**, *21*, 214–221. [CrossRef]

26. Xu, W.; Jiang, Y.; Ren, X. Combustion promotion and extinction of premixed counterflow methane/air flames by $C_6F_{12}O$ fire suppressant. *J. Fire Sci.* **2016**, *34*, 289–304. [CrossRef]

27. Xu, W.; Jiang, Y.; Qiu, R.; Ren, X. Influence of Halon replacements on laminar flame speed and extinction stretch rate of hydrocarbon flames. *Combust. Flame* **2017**, *182*, 1–13. [CrossRef]

28. Gibbs, G.J.; Calcote, H.F. Effect of molecular structure on burning velocity. *J. Chem. Eng. Data.* **1959**, *4*, 226–237. [CrossRef]

29. Qin, X.; Kobayashi, H.; Niioka, T. Laminar burning velocity of hydrogen–air premixed flames at elevated pressure. *Exp. Therm. Fluid. Sci.* **2000**, *21*, 58–63. [CrossRef]

30. Dagaut, P.; Karsenty, F.; Dayma, G.; Diévart, P.; Hadj-Ali, K.; Mzé-Ahmed, A.; Braun-Unkhoff, M.; Herzler, J.; Kathrotia, T.; Kick, T.; et al. Experimental and detailed kinetic model for the oxidation of a Gas to Liquid (GtL) jet fuel. *Combust. Flame* **2014**, *161*, 835–847. [CrossRef]

31. Pareja, J.; Burbano, H.J.; Ogami, Y. Measurements of the laminar burning velocity of hydrogen–air premixed flames. *Int. J. Hydrogen Energy* **2010**, *35*, 1812–1818. [CrossRef]

32. Natarajan, J.; Lieuwen, T.; Seitzman, J. Laminar flame speeds of H_2/CO mixtures: Effect of CO_2 dilution, preheat temperature, and pressure. *Combust. Flame* **2007**, *151*, 104–119. [CrossRef]

33. Lapalme, D.; Seers, P. Influence of CO_2, CH_4, and initial temperature on H_2/CO laminar flame speed. *Int. J. Hydrogen Energy* **2014**, *39*, 3477–3486. [CrossRef]

34. Lewis, B.; Von Elbe, G. *Combustions, Flames and Explosions of Gases*, 3rd ed.; Academic Press: Cambridge, UK, 1987.

35. Mazas, A.N.; Fiorina, B.; Lacoste, D.A.; Schuller, T. Effects of water vapor addition on the laminar burning velocity of oxygen-enriched methane flames. *Combust. Flame* **2011**, *158*, 2428–2440. [CrossRef]

36. Dong, C.; Zhou, Q.; Zhao, Q.; Zhang, Y.; Xu, T.; Hui, S. Experimental study on the laminar flame speed of hydrogen/carbon monoxide/air mixtures. *Fuel* **2009**, *88*, 1858–1863. [CrossRef]

37. Lee, M.; Ranganathan, S.; Rangwala, A.S. Influence of the reactant temperature on particle entrained laminar methane–air premixed flames. *Proc. Combust. Inst.* **2015**, *35*, 729–736. [CrossRef]

38. Moffat, R.J. Describing the uncertainties in experimental results. *Exp. Therm. Fluid. Sci.* **1988**, *1*, 3–17. [CrossRef]

39. Tang, Y.; Kong, C.; Zong, Y.; Li, S.; Zhuo, J.; Yao, Q. Combustion of aluminum nanoparticle agglomerates: From mild oxidation to microexplosion. *Proc. Combust. Inst.* **2017**, *36*, 2325–2332. [CrossRef]

40. Gu, X.J.; Haq, M.Z.; Lawes, M.; Woolley, R. Laminar burning velocity and markstein lengths of methane-air mixtures. *Combust. Flame* **2000**, *121*, 41–58. [CrossRef]

41. Hassan, M.I.; Aung, K.T.; Faeth, G.M. Measured and predicted properties of laminar premixed methane-air flames at various pressures. *Combust. Flame* **1998**, *115*, 539–550. [CrossRef]

42. Rozenchan, G.; Zhu, D.L.; Law, C.K.; Tse, S.D. Outward propagation, burning velocities, and chemical effects of methane flames up to 60 atm. *Proc. Combust. Inst.* **2002**, *29*, 1461–1469. [CrossRef]

43. Vagelopoulos, C.M.; Egolfopoulos, F.N. Direct experimental determination of laminar flame speeds. *Symp. (Int.) Combust.* **1998**, *27*, 513–519. [CrossRef]

44. Bosschaart, K.J.; De Goey, L.P.H. The laminar burning velocity of flames propagating in mixtures of hydrocarbons and air measured with the heat flux method. *Combust. Flame* **2004**, *136*, 261–269. [CrossRef]

45. Soo, M.; Julien, P.; Goroshin, S.; Bergthorson, J.M.; Frost, D.L. Stabilized flames in hybrid aluminum-methane-air mixtures. *Proc. Combust. Inst.* **2013**, *34*, 2213–2220. [CrossRef]